

Multiaxial Fatigue Life Prediction Methods for Notched Bars of Ti-6Al-4V

Dr. Alan Kallmeyer¹, Mr. Ahmo Krgo¹, and Dr. Peter Kurath²

¹ Department of Mechanical Engineering, North Dakota State University, Fargo, ND

² Department of Mechanical Engineering, University of Illinois, Urbana, IL

ABSTRACT

Many critical engineering components are routinely subjected to cyclic multiaxial stress states, which may include non-proportional loading and multidimensional mean stresses. Initial efforts by the authors involved the identification of suitable multiaxial damage parameters for a Ti-6Al-4V titanium alloy utilizing smooth samples. As with uniaxial loading, the extension of the multiaxial data to a notched geometry poses challenges. Utilizing the multiaxial stress-strain state at the notch root, estimates of the fatigue life for multiaxially loaded notched members may be highly conservative, even for damage parameters that successfully modeled the smooth specimens under identical loading. By using an “average” of the multiaxial stress field over a small region near the notch in the calculation of the damage parameters, more realistic fatigue life estimates were obtained.

INTRODUCTION

Performance requirements in certain applications require that an adequate fatigue damage parameter be identified, rather than masking uncertainty in excessive factors of safety. Ideally, uniaxial data would be utilized to establish a baseline data set that could be extended to more complex loading with a multiaxial damage parameter. A previous investigation [1] scrutinized twenty-two existing fatigue damage parameters in light of approximately thirty multiaxial smooth bar tests which encompassed a variety of mean stress conditions and non-proportionality. Figure 1 highlights some of the non-proportional paths employed in the investigation. Both the level of loading and shape of the paths are intended to simplify portions of actual service events. The reader is referred to reference [1] for other details of the testing and specimen design.

The parameters evaluated in reference [1] included both the scalar effective-stress type as well as the more recently introduced critical plane approaches. For the most part, any plastic deformation observed during the multiaxial testing was restricted to the first reversal, resulting in fatigue lives of 5×10^4 to 5×10^6 cycles. Only one effective-stress type parameter, the modified Manson-McKnight parameter [2, 3], showed promise for general multiaxial loading. This model uses an alternating stress range, $\Delta\sigma_{eff}$, defined from the general form of effective stress with the range of each stress component, and an effective mean stress, σ_{eff}^{mean} , defined as the effective mean stress obtained using the mean stress for each component.

$$Damage = \frac{1}{2} \Delta\sigma_{eff}^{(w-1)} \sigma_{max}^w, \quad \sigma_{max} = \frac{\Delta\sigma_{eff}}{2} + \frac{\beta}{2} \sigma_{eff}^{mean}, \quad \beta = \frac{(\sum \sigma_1 + \sum \sigma_3)}{(\sum \sigma_1 - \sum \sigma_3)} \quad (1)$$

The sign and magnitude of the mean stress term in the model is modified by multiplying the effective mean by the term $\beta/2$. β is defined by $\sum \sigma_1$ and $\sum \sigma_3$, which are the sums of the first and third principal stresses, respectively, at the maximum and minimum points in the cycle. Then σ_{max} is obtained by adding the effective stress amplitude to the modified mean stress term. If

strains (rather than stresses) are known, a “pseudo-stress” range is defined that makes use of an effective strain range with an elastic Poisson’s ratio multiplied by the linear modulus to obtain $\Delta\sigma_{\text{eff}}$.

Three critical plane models were identified [1] for extension to notched member analysis. They include the Findley [4] parameter, which modifies the maximum shear amplitude by the maximum stress normal to the orientation of maximum shear multiplied by an influence factor, k . While it has been shown that k may not be a constant, it is assumed to be for the life range under consideration.

$$Damage = \frac{\Delta\tau}{2} + k \sigma_n^{\text{max}} \quad (2)$$

The Fatemi-Socie-Kurath (FSK) [5, 6] parameter has a similar basic mechanistic interpretation, but is formulated in terms of the shear strain amplitude.

$$Damage = \frac{\Delta\gamma}{2} (1 + k \sigma_n^{\text{max}}) \quad (3)$$

Finally, a modification of the Chu-Conle-Bonnen (CCB) [7] parameter showed promise. It may be interpreted as a modification of the Smith-Watson-Topper (SWT) parameter, in which a shear term ($\Delta\gamma \tau_{\text{max}}$) has been added to the normal stress-strain term. This parameter can be considered to represent the strain energy acting on a plane, as it involves the multiplication of corresponding stress and strain components, if all stress components other than axial and shear stress are zero. This is true for axial-torsional loading of thin walled tubes or elastic solid round bars. For more generalized multiaxial loading, the interpretation must be that of a portion of the strain energy. In this study, a slight modification was made to the model by multiplying the second term ($\Delta\varepsilon \sigma_{\text{max}}/2$) by an empirical factor, k , to allow for an adjustment in the influence of this term. It was found that this modification significantly improved the accuracy of this model.

$$Damage = \Delta\gamma \tau_{\text{max}} + k \frac{\Delta\varepsilon}{2} \sigma_n^{\text{max}} \quad (4)$$

The SWT parameter itself was also previously considered [1] as a critical plane parameter. However, comparison of this model with the smooth-bar multiaxial data showed it was highly non-conservative. The successful critical plane parameters were all based on alternating shear stress or strain terms, indicating that shear stresses/strains drive the formation of fatigue cracks in this material.

Interpretation of the basic form of Equations (1-4) is debatable from a mechanistic viewpoint for non-proportional loading. In this research, the maximum damage orientation is defined as that which has the maximum value of the parameter. While for more complex loading, the identification of a cycle, and the ancillary terms associated with that event pose challenges, the current efforts consider the basic path (Fig. 1) to be the fatigue event or cycle. For more complex loading, the fact that the critical plane may differ from event to event has implications regarding cumulative damage, which will not be addressed in this investigation.

Damage for the more statistically significant uniaxial data has been fit to the following base equation for each parameter.

$$Damage = A(N_f)^b + C(N_f)^d \quad (5)$$

It is emphasized that the coefficients and exponents are not the traditional strain-life constants. Uniaxial data at different load ratios were utilized to calculate the value of k or w for each parameter. The solid curves shown in any of the life figures are the fit of the uniaxial data, utilizing Eq. (5). The constants determined for each parameter are summarized in Table 1. Smooth specimen multiaxial results are summarized in Figures 2 through 5 for the aforementioned parameters. There are approximately eight additional data points not reported in reference [1], that are summarized in Table 2.

Statistical comparison of the baseline multiaxial results is presented in Table 3 utilizing the following equation.

$$\% Error = \frac{Damage_{experiment} - Damage_{predicted}}{Damage_{experiment}} \times 100 \quad (6)$$

Using this method of comparison, the mean value of the percent error indicates the degree of offset of the predicted damage parameters for the multiaxial data, relative to the baseline uniaxial curve. The standard deviation provides a relative measure of the degree of scatter about the curve. An ideal model is one for which both the mean and standard deviation of the error are minimized.

NOTCHED EXPERIMENTAL PROGRAM

Five circumferentially notched round bars with a notch net section diameter of 12.5 mm, a notch depth of 3.25 mm, and a notch radius of 2.5 mm were tested using the load paths shown in Figure 6. Theoretical stress concentration factors of $K_{\sigma} = 1.85$ and $K_{\tau} = 1.35$ are associated with this geometry [8]. Specimen preparation was identical to the uniaxial and multiaxial smooth specimens tested previously. Individual test data are summarized in Table 4.

NOTCH ANALYSIS AND DISCUSSION

Since strains could not be measured at the notch root, a finite element analysis was performed to determine the stress-strain state at the notch. ANSYS was utilized with a tetrahedral 10-node element. A sensitivity analysis was conducted to ensure convergence of the stress solutions, using meshes that varied from approximately 5,000 to over 17,000 elements for the entire specimen. In the final mesh, shown in Figure 7, the average element side length in the notch root was approximately 0.5 mm. The results of the elastic analyses indicated that one of the tests (test C in Table 4) experienced plastic deformation during the loading. Consequently, an elastic-plastic analysis was conducted in ANSYS for this case. In performing the elastic-plastic analysis, a multilinear kinematic hardening rule was assumed. The Ramberg-Osgood relation was used to model the cyclic stress-strain curve, using the data obtained from uniaxial testing. The material properties used in this analysis are $E = 116.3$ GPa, $\nu = 0.349$, $K' = 855$ MPa, and $n' = 0.0149$. Figure 7 shows a typical von Mises contour stress plot for test A, while Figure 8 shows the stress components as a function of radial position through the notch section for tests A and C. These stress components were used to calculate a value for each damage parameter. Again, it was assumed any plastic deformation was restricted to the first reversal.

Even with uniaxial notches, knowledge of the theoretical stress concentration factor often renders conservative life estimates. This led to the development of fatigue stress concentration factors, K_f , and the concept of a notch sensitivity factor, q . These developments are summarized

in reference [9]. In general, the sharper a notch, the higher the stress concentration factor, and the steeper the elastic stress-strain gradient. In essence, these concepts assume the maximum principal stress or strain is the relevant damage parameter and serve to reduce the maximum value of the damage parameter. As previously mentioned, the damage parameters identified in this study that provided some measure of correlation for the multiaxial data can at least conceptually be considered shear based. As such, the constraint inherent in a circumferentially notched round specimen would lead the maximum principal stress concepts to overestimate the effect of the notch. Slavic [2] and Taylor [10] acknowledge that notches may not be as severe as anticipated, and postulate some critical region over which the damage should be considered.

Figures 9 through 12 show the radial damage predicted for each damage algorithm utilizing the individual stress-strain components determined from the finite element analysis. The solid point on each curve shows the location of the damage parameter calculated using the experimental life and the baseline damage curve. The fact that these points are all located subsurface indicates that the damage predicted employing surface stresses and strains is conservative. They also render some insight as to a depth over which the damage needs to be assessed. Using 0.05 mm increments, the subsurface damage was calculated, and Eq. (6) was utilized to calculate a percent error for each test. The optimized depth, which best correlates all the notched specimen data to the uniaxial baseline curve, was chosen to minimize the percent error. In other words, the mean of the notched data was chosen to correspond to the baseline uniaxial data. These results, along with the surface damage calculations, are shown in Figures 13 through 16 (left plot) for each of the damage parameters under consideration.

Notch acuity was shown to be influential in uniaxial experiments and theories previously presented. The observation that, in these tests, the torsional and axial stress concentrations differ could cause some of the “depth” discrepancy observed here. Depending on the parameter evaluated, the optimal “damage depth” varied from 0.25 mm to 0.45 mm. While these dimensions seem large compared to prior values assigned in the literature, it should be noted that the stress concentration factors in the current experiments were lower than most considered in the literature. The low value of K_t also tends to cause the stress-strain gradient to shallow, but cover a significant portion of the net section of the specimen (Fig. 8). Hence, the dimensions cited here should be interpreted in the context of the geometry of notches tested.

Rather than assign a specific depth value to the damage, a third methodology involves integrating the value of the damage parameter over a depth beneath the surface, r^* , to obtain an averaged damage.

$$\overline{Damage} = \frac{1}{r^*} \int_{r_o - r^*}^{r_o} (Damage) dr \quad (7)$$

where r_o is the outer radius at the notch section. The results of this analysis are presented in Figures 13 through 16 (right plot), and closely resemble the results of the point-depth analysis. A similar increment in depth and methodology to place the mean notched life on the uniaxial baseline curve was employed in this analysis. The range of depths, or r^* , ranged from 0.4 mm with the modified Manson-McKnight parameter to 1.2 mm for the Fatemi-Socie-Kurath parameter. Again these are somewhat higher than those reported in the literature. A statistical comparison of the point and line depth averaging techniques is summarized in Table 5. As before, lower values of the mean and standard deviation are desirable.

While the line averaged results look similar to the point results, the line average method has the conceptual advantage of somewhat accounting for the differences in axial and torsional stress concentration factors that result in different stress and strain gradients. The stress state of the geometry tested is two dimensional at the surface, but three dimensional below the surface. Neglecting the circumferential stress would have introduced significant errors in the calculations, but the effects of the radial stress below the surface were negligible. Due to the symmetry of the loading and stress state near the notch, the critical plane orientation remained approximately constant over the depths considered here. For more complex loading and a general geometry, an averaging scheme over a "critical" volume of dimension V^* may be required. However, it seems that averaging or integrating the value of the damage parameter has inherent advantages over modifying the stress-strain state, especially for more complex loading. A major drawback at this juncture is that no overall methodology has been forwarded to determine the critical distance, line length or volume for a general multiaxial loading and geometry.

CONCLUSIONS

As with uniaxial loading, the theoretical stress concentration factors overestimate the effects of fatigue for multiaxial loading. The Findley critical plane approach provided the best overall representation of the smooth bar data, and also for the notched specimen data using the line averaging technique. Empirical determination of the depth or line length for averaging needs to be refined.

ACKNOWLEDGMENT

This work was supported under Air Force Contract No. F49620-99-C-0007, Advanced High Cycle Fatigue Life Assurance Methodologies, with Dr. Jeffrey Calcatera, AFRL/MLLM, Project Monitor. The contract is being administrated through the University of Dayton Research Institute under subcontracts RSC99013 with North Dakota State University and RSC98007 with the University of Illinois.

REFERENCES

1. Krgo, A., Kallmeyer, A. R., and Kurath, P., "Evaluation of HCF Multiaxial Fatigue Life Prediction Methodologies for Ti-6Al-4V," Proceedings of the 5th National Turbine Engine High Cycle Fatigue Conference, Arizona, 2000.
2. Slavic, D. C., Duniak, T., Griffiths, J., and Kurath, P., "Fatigue Crack Initiation Modeling in Ti-6Al-4V for Smooth and Notched Geometries," Proceedings of the 5th National Turbine Engine High Cycle Fatigue Conference, Arizona, 2000.
3. McKnight, R. L. and Slavik, D. C., General Electric Aircraft Engines, personal communication, 2000.
4. Findley, W. N., "Fatigue of Metals Under Combinations of Stresses," *Transactions*, ASME, Vol. 79, 1957, pp. 1337-1348.
5. Fatemi, A. and Socie, D. F., "A Critical Plane Approach to Multiaxial Damage Including Out-of-Phase Loadings," *Journal of Fatigue and Fracture of Engineering Materials and Structures*, Vol. 11, No. 3, pp. 149-165, 1988.
6. Kurath, P. and Fatemi, A., "Cracking Mechanisms for Mean-Stress/Strain Low Cycle Multiaxial Fatigue Loadings," *Quantitative Methods in Fractography*, ASTM STP 1085, B.

- M. Strauss and S. K. Putatunda, Eds., American Society for Testing and Materials, Philadelphia, PA, pp. 123-143, 1990.
7. Chu, C. C., Conle, F. A., and Bonnen, J. J. F., "Multiaxial Stress-Strain Modeling and Fatigue Life Prediction of SAE Axle Shafts," *Advances in Multiaxial Fatigue*, ASTM STP 1191, D. L. McDowell and R. Ellis, Eds., American Society for Testing and Materials, Philadelphia, pp. 37-54, 1993.
 8. Peterson, R. E. *Stress Concentration Factors*, Wiley Interscience, 1974.
 9. Peterson, R. E., Chapter 13, *Metal Fatigue*, Sines & Waisman, Eds., McGraw-Hill, 1959.
 10. Taylor, D., "Geometrical Effects in Fatigue: A Unifying Theoretical Model," *International Journal of Fatigue*, Vol. 21, pp. 413-420, 1999.

TABLES AND FIGURES

Table 1
Curve-Fit Constants to Uniaxial Data

Model	A (ksi)	b	C (ksi)	d	k or w
Modified Manson-McKnight	7611	-0.6471	65.39	-0.03582	0.433
Findley	15,907	-0.7368	69.2	-0.03959	0.35
Fatemi-Socie-Kurath	7.54	-0.6467	0.01264	-0.02647	6.0
Modified Chu-Conle-Bonnen	424.4	-0.6475	0.676	-0.03152	2.7

Table 2
Additional Biaxial (Smooth Specimen) Data

Spec. ID	Test Description	$\Delta\gamma$ (%)	$\Delta\varepsilon$ (%)	N_f (cycles)
142-5	$R = -1$ torsion	1.22	0	260,657
178-3	$R = -1$ torsion	1.12	0	843,404
142-9	$R = 0.1$ torsion	1.12	0	184,669
142-8	$R_\varepsilon = R_\gamma = -1$ box path	0.82	0.60	59,432
178-7	$R_\varepsilon = R_\gamma = -1$ box path	0.82	0.60	72,360
142-11	$R_\varepsilon = -3, R_\gamma = -1$ box path	0.82	0.60	182,149
178-8	$R_\varepsilon = -3, R_\gamma = -1$ box path	0.82	0.60	212,337
178-12	Check path	1.22	0.30	50,568

Table 3
Statistical Comparison of Multiaxial Models for Smooth Specimen Data

Model	Uniaxial Data (% Error)		Biaxial Data (% Error)	
	Mean	St. Dev.	Mean	St. Dev.
Modified Manson-McKnight	-0.54	7.51	-5.91	11.75
Findley	-0.68	8.37	-0.15	9.36
Fatemi, Socie, Kurath	-2.42	16.27	2.86	12.25
Modified Chu, Conle, Bonnen	-2.47	17.26	1.36	19.03

Table 4
Notched Specimen Test Conditions and Fatigue Lives

Spec/Path	P_{max} (lb)	P_{min} (lb)	T_{max} (lb-in)	T_{min} (lb-in)	N_f (cycles)
132-4/A	2000	2000	750	-750	369,700
132-3/B	-2000	-2000	750	-750	$>1.8 \times 10^6$
132-1/C	0	0	1500	75	627,000
132-2/D	9000	1000	750	90	123,800
132-5/E	6500	-6500	550	-550	416,200

Table 5
Statistical Comparison of Multiaxial Models for Notched Specimen Data

Model	DP calculated at notch root surface (% Error)		DP calculated at critical depth (% Error)		DP averaged over critical length (% Error)	
	Mean	St. Dev.	Mean	St. Dev.	Mean	St. Dev.
Mod. M-M	8.84	8.47	0.51	11.24	0.043	10.45
Findley	16.3	6.39	0.47	7.44	1.1	8.06
FSK	32.04	12.77	-0.67	20.93	-0.75	19.39
Mod. CCB	31.06	12.45	0.003	18.84	-1.37	21.69

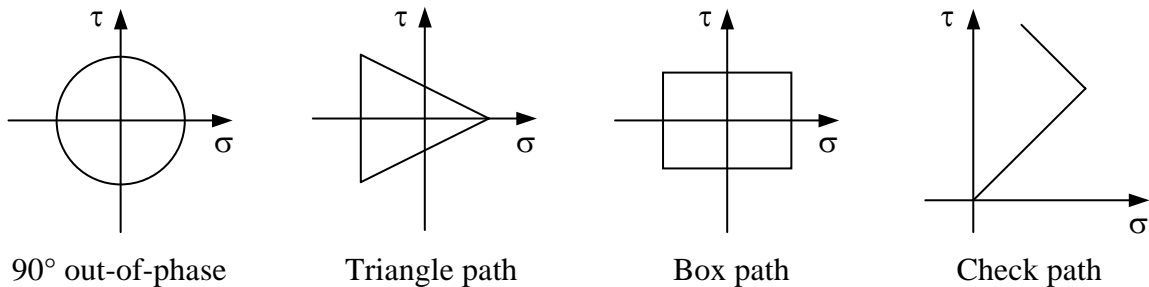
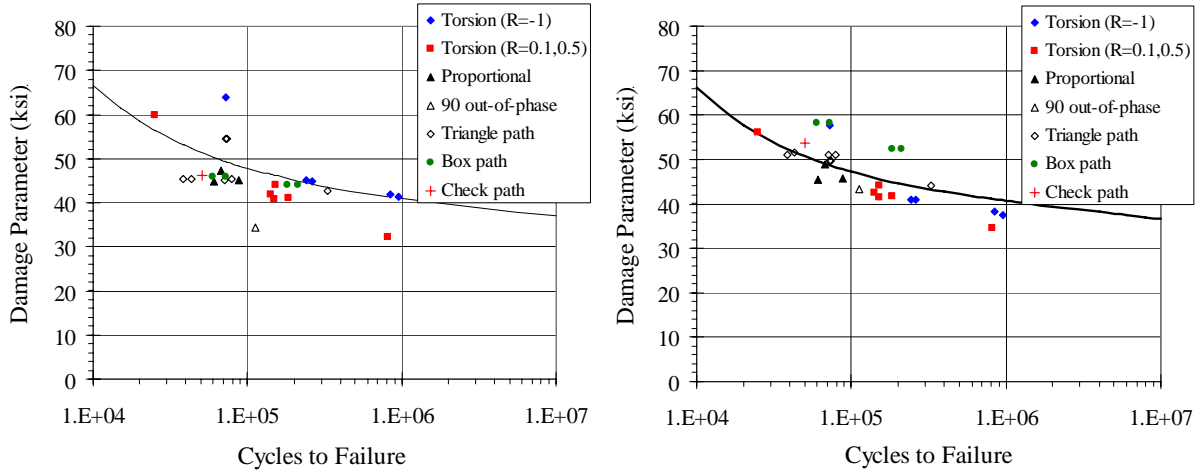
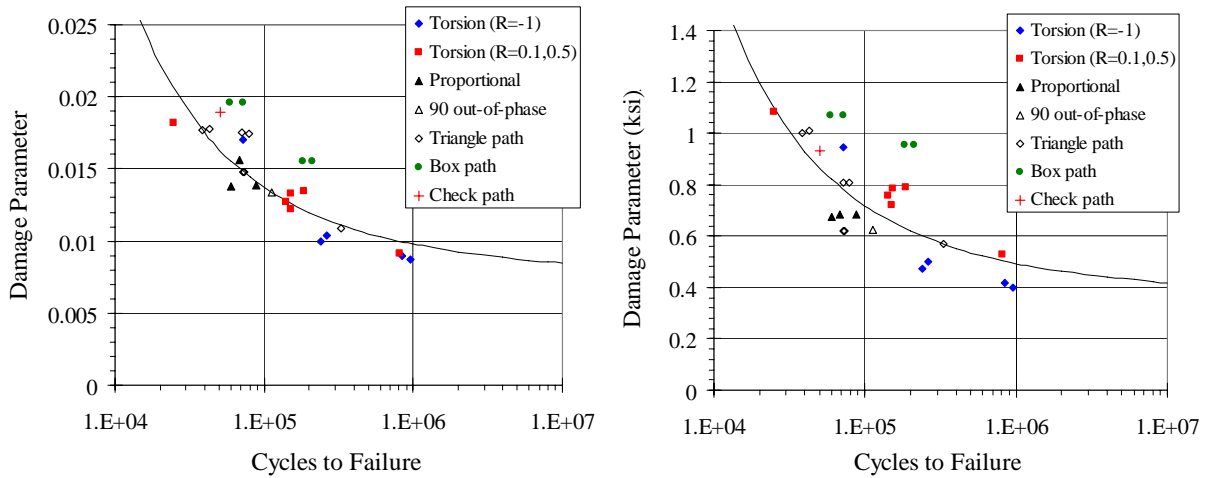


Figure 1. Non-proportional load paths for smooth biaxial tests.



Figures 2 & 3. Damage parameter vs. life curves for modified Manson-McKnight (left) and Findley models (right), showing smooth biaxial data (curves represent uniaxial data).



Figures 4 & 5. Damage parameter vs. life curves for Fatemi-Socie-Kurath (left) and modified Chu-Conle-Bonnen models (right), showing smooth biaxial data (curves represent uniaxial data).

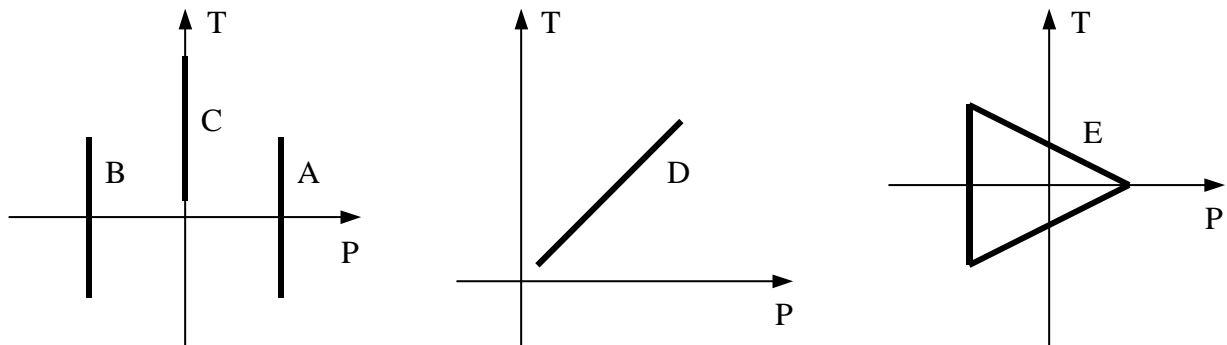


Figure 6. Load paths for notched specimen tests.

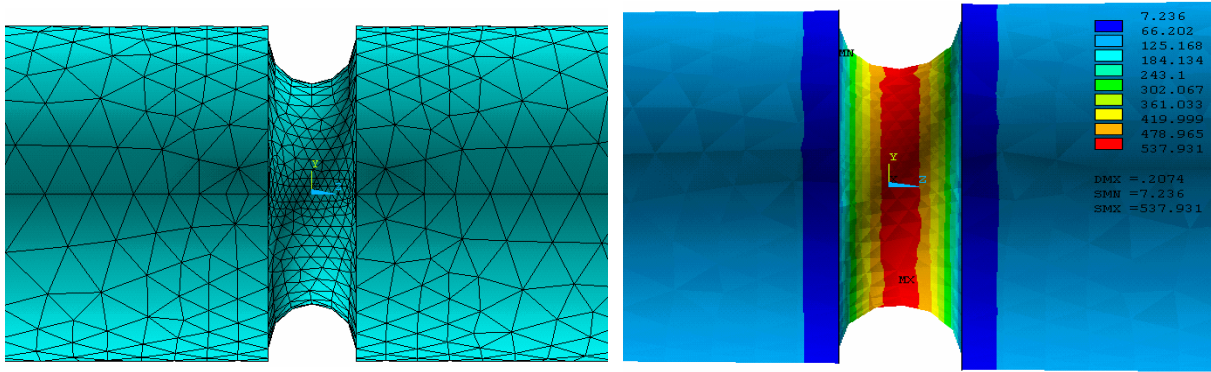


Figure 7. Finite element mesh of notched specimen, and sample plot of von Mises stress distribution (test A).

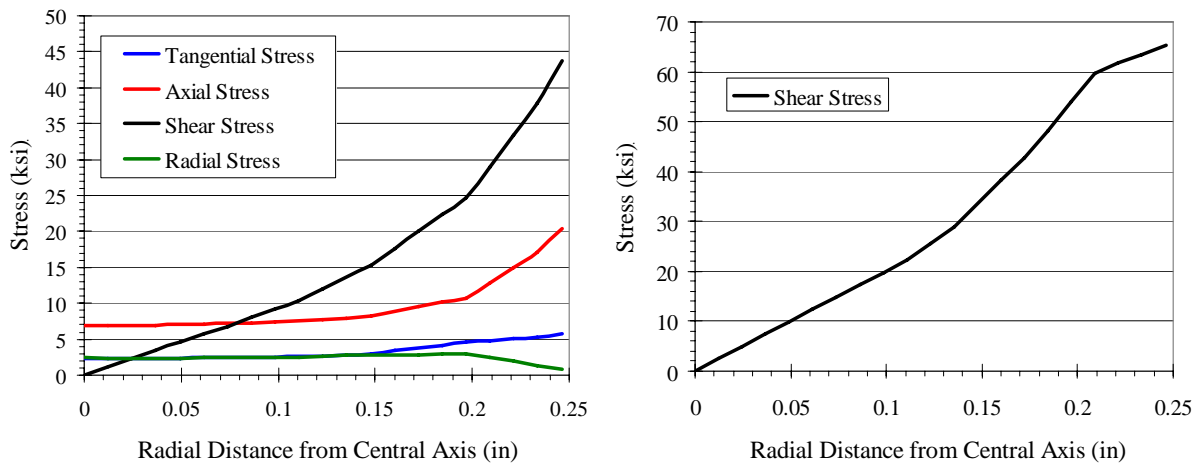
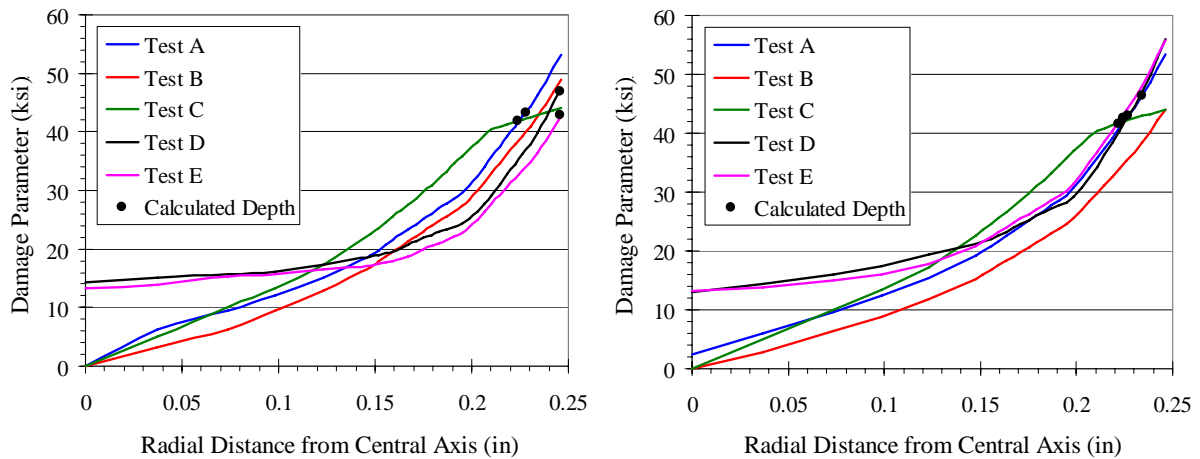
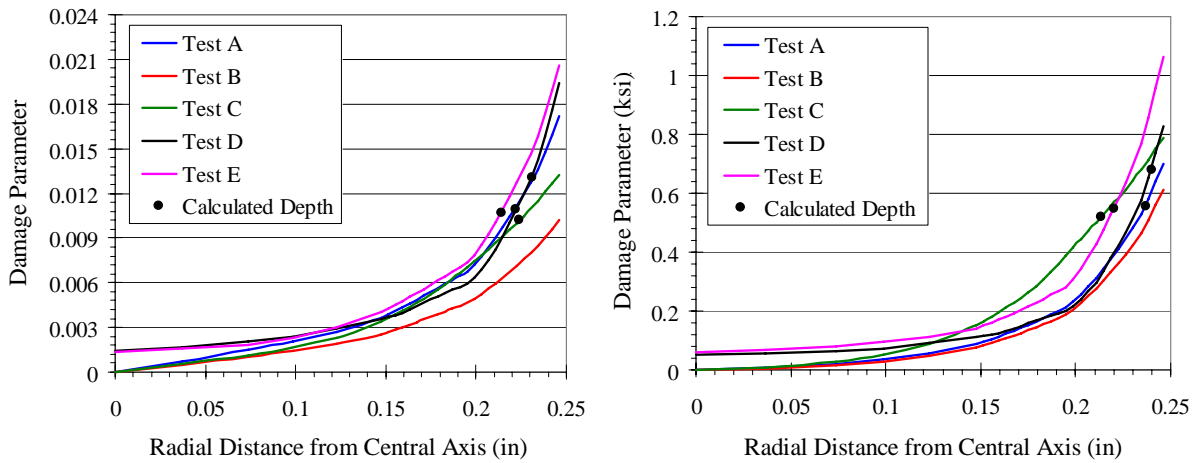


Figure 8. Plots of stress distribution vs. depth under the notch for tests A (left) and C (right).



Figures 9 & 10. Damage parameter vs. depth under notch for modified Manson-McKnight (left) and Findley models (right), and depth at which damage parameters correspond with experimental lives.



Figures 11 & 12. Damage parameter vs. depth under notch for Fatemi-Socie-Kurath (left) and modified Chu-Conle-Bonnen models (right), and depth at which damage parameters correspond with experimental lives.

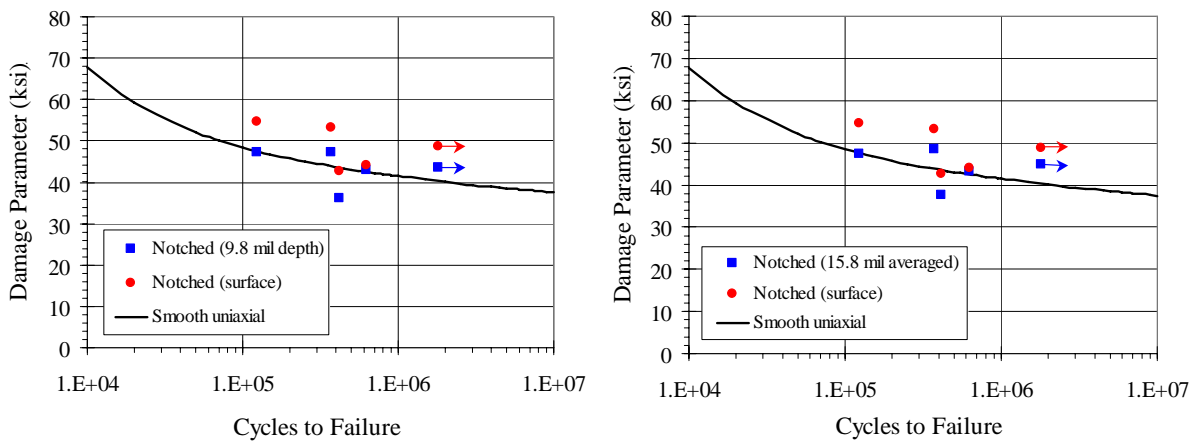


Figure 13. Comparison of damage parameters from modified Manson-McKnight model calculated at surface, at depth of 9.8 mil (0.25 mm), and averaged over 15.8 mil (0.4 mm) depth.

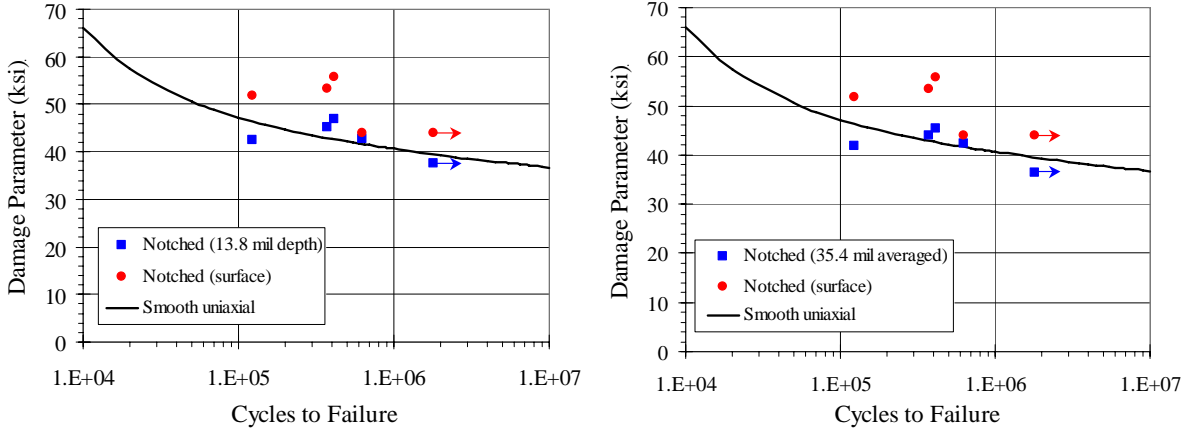


Figure 14. Comparison of damage parameters from Findley model calculated at surface, at depth of 13.8 mil (0.35 mm), and averaged over 35.4 mil (0.9 mm) depth.

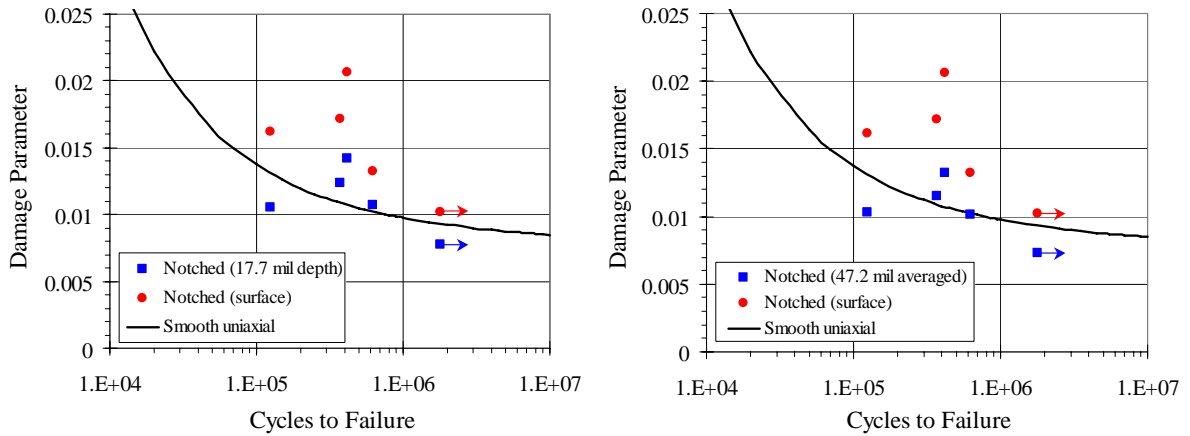


Figure 15. Comparison of damage parameters from Fatemi-Socie-Kurath model calculated at surface, at depth of 17.7 mil (0.45 mm), and averaged over 47.2 mil (1.2 mm) depth.

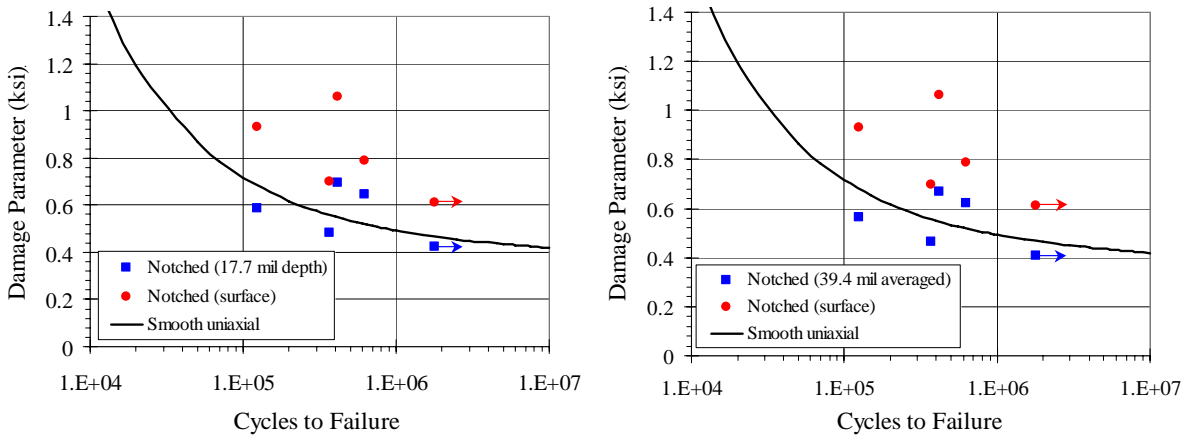


Figure 16. Comparison of damage parameters from modified Chu-Conle-Bonnen model calculated at surface, at depth of 17.7 mil (0.45 mm), and averaged over 39.4 mil (1 mm) depth.